

Integrating the IMSA With a New Integral Equation Method for Imaging Strong Scatterers

M. Salucci, A. Polo, and A. Massa

Abstract

In this work, an innovative inverse scattering (*IS*) methodology is proposed. The developed technique relies on the suitable integration of the iterative multi-scaling approach (*IMSA*) and a New Integral Equation (*NIE*) strategy. One the one hand, the *IMSA* allows to effectively tackle both non-linearity and ill-posedness of the *IS* problem thanks to the adaptive refinement of the resolution only within the detected region-of-interest and the exploitation of *progressively-acquired* information on the solution. On the other hand, the qualitative imaging of strong scatterers is enabled thanks to the *NIE*, allowing to reformulate the main equations modeling the physics of the problem such that it is possible to reduce its non-linearity and reduce the occurrence of false solutions. Preliminary numerical results are provided to demonstrate the effectiveness of the proposed *IMSA-NIE* methodology.

Contents

1 List of Symbols	2
2 Mathematical Formulation	3
2.1 Contrast Function and Contrast Source	3
2.2 <i>NIE</i> Formulation of the Scattering Problem [17]	3
2.2.1 Discretized Version	4
2.3 Reconstruction Error	5
2.4 Signal to Noise Ratio	5
2.5 Degrees of Freedom (<i>DoFs</i>) of the Scattered Field	6
2.6 <i>IMSA – SOM – NIE</i> Method	7
2.6.1 Stopping Criteria	7
2.6.2 Adaptive Selection of the Number of Singular Values	7
2.7 Adaptive Computation of the <i>NIE</i> Regularization Parameter	7
3 Preliminary Software Validation	8
3.1 Goal	8
3.2 Parameters	9
3.3 Results	11
3.4 Conclusions	13

1 List of Symbols

- $k = \frac{2\pi}{\lambda}$: Free-space wave-number;
- D : Investigation domain;
- L_D : Side of the investigation domain;
- $a = L_D \frac{\sqrt{2}}{2}$: Radius of the smallest circle containing D ;
- $\mathbf{r} = (x, y)$: Position vector;
- $\tau(\mathbf{r})$: Contrast function;
- $\varepsilon_r(\mathbf{r})$: Relative permittivity;
- ε_0 : Free-space permittivity;
- $\sigma(\mathbf{r})$: Conductivity;
- Ξ : Reconstruction error;
- V : Number of views/sources;
- φ^v : Direction of the v -th plane wave ($v = 1, \dots, V$);
- M : Number of measurement points;
- ρ : Radius of the measurement domain;
- N : Number of discretization cells inside D ;
- Γ : Number of degrees-of-freedom of the scattered field;
- U : Number of retrievable unknowns;
- η : *IMSA* Stopping threshold;
- S : Maximum number of *IMSA* iterations;
- $L^{(s)}$: Side of the region of interest (*RoI*) at the s -th *IMSA* step ($s = 1, \dots, S$);
- K : Number of singular values used by the *SOM* to retrieve the minimum-norm currents;
- α : Threshold for the adaptive selection of the number of singular values;
- χ_m : m -th Singular value of the scattering operator ($m = 1, \dots, M$);
- MF : Number of Fourier bases;
- β : *NIE* regularization parameter;
- γ : Multiplicative factor for the adaptive computation of β ;
- I : Number of iterations;

2 Mathematical Formulation

2.1 Contrast Function and Contrast Source

The contrast function at position $\mathbf{r} = (x, y) \in D$ is defined as [1]

$$\tau(\mathbf{r}) = \Re\{\tau(\mathbf{r})\} + j\Im\{\tau(\mathbf{r})\} = [\varepsilon_r(\mathbf{r}) - 1] - j \left[\frac{\sigma(\mathbf{r})}{2\pi f \varepsilon_0} \right]; \quad \mathbf{r} \in D \quad (1)$$

The contrast source is defined as

$$J(\mathbf{r}) = \tau(\mathbf{r}) E(\mathbf{r}); \quad \mathbf{r} \in D \quad (2)$$

2.2 NIE Formulation of the Scattering Problem [17]

Assuming a 2 – D investigation domain D with background permittivity and permeability ε_0 and μ_0 , respectively, the standard Lippmann-Schwinger integral equation ($LS - IE$) describes the total electric field inside D as follows

$$E(\mathbf{r}) = E^{inc}(\mathbf{r}) + \int_D G(\mathbf{r}, \mathbf{r}') \tau(\mathbf{r}') E(\mathbf{r}') d\mathbf{r}'; \quad \mathbf{r} \in D \quad (3)$$

or equivalently as

$$J(\mathbf{r}) = \tau(\mathbf{r}) E^{inc}(\mathbf{r}) + \tau(\mathbf{r}) \int_D G(\mathbf{r}, \mathbf{r}') J(\mathbf{r}') d\mathbf{r}'; \quad \mathbf{r} \in D. \quad (4)$$

Moreover, the scattered field is given by

$$E^{sca}(\mathbf{r}) = \int_D G(\mathbf{r}, \mathbf{r}') J(\mathbf{r}') d\mathbf{r}'. \quad (5)$$

By multiplying both sides of (4) by a function

$$\beta(\mathbf{r}) [\beta(\mathbf{r}) \tau(\mathbf{r}) + 1]^{-1} \quad (6)$$

it is possible to obtain the following *NIE* equation

$$\beta(\mathbf{r}) J(\mathbf{r}) = R(\mathbf{r}) \beta(\mathbf{r}) J(\mathbf{r}) + R(\mathbf{r}) \left[E^{inc}(\mathbf{r}) + \int_D G(\mathbf{r}, \mathbf{r}') J(\mathbf{r}') d\mathbf{r}' \right]; \quad \mathbf{r} \in D \quad (7)$$

where

$$R(\mathbf{r}) = \beta(\mathbf{r}) \tau(\mathbf{r}) [\beta(\mathbf{r}) \tau(\mathbf{r}) + 1]^{-1} \quad (8)$$

is the modified contrast function and $\beta(\mathbf{r})$ is a local regularization parameter. The only condition to be satisfied by $\beta(\mathbf{r})$ is that

$$\beta(\mathbf{r}) \tau(\mathbf{r}) + 1 \neq 1; \quad \mathbf{r} \in D \quad (9)$$

Moreover, since the scatterer could be in every position within D , a constant value for $\beta(\mathbf{r})$ is chosen, i.e.,

$$\beta(\mathbf{r}) = \beta_0; \quad \mathbf{r} \in D \quad (10)$$

2.2.1 Discretized Version

By partitioning D into N sub-domains, and assuming the illumination by V sources, the $LS - IE$ eq. (4) becomes

$$\underline{J}_v = \underline{\tau} \left[\underline{E}_v^{inc} + \underline{G}_{int} \underline{J}_v \right]; \quad v = 1, \dots, V \quad (11)$$

where

$$\underline{J}_v = \{J_v(\mathbf{r}_n); \quad n = 1, \dots, N\}^T \quad (12)$$

$$\underline{E}_v^{inc} = \{E_v^{inc}(\mathbf{r}_n); \quad n = 1, \dots, N\}^T \quad (13)$$

$$\underline{\tau} = \begin{bmatrix} \tau(\mathbf{r}_1) & 0 & \cdots & 0 \\ 0 & \tau(\mathbf{r}_2) & & \vdots \\ \vdots & & \ddots & \vdots \\ 0 & \cdots & \cdots & \tau(\mathbf{r}_N) \end{bmatrix}. \quad (14)$$

On the other hand, the NIE eq. (7) can be discretized as follows

$$\beta_0 \underline{J}_v = \underline{R} \left[\beta_0 \underline{J}_v + \underline{E}_v^{inc} + \underline{G}_{int} \underline{J}_v \right]; \quad v = 1, \dots, V \quad (15)$$

where

$$\underline{R} = \beta_0 \underline{\tau} [\beta_0 \underline{\tau} + 1]^{-1}. \quad (16)$$

2.3 Reconstruction Error

The following integral error is defined and used to evaluate the quality of the retrieved solutions

$$\Xi_{reg} = \frac{1}{N_{reg}} \sum_{n=1}^{N_{reg}} \frac{|\tau_n - \tilde{\tau}_n|}{|\tau_n + 1|} \quad (17)$$

where τ_n and $\tilde{\tau}_n$ are the actual and retrieved contrast for the n -th cell, respectively, and reg indicates if the error computation covers

- the overall investigation domain ($reg \Rightarrow tot$),
- the actual scatterer support ($reg \Rightarrow int$),
- the background region ($reg \Rightarrow ext$).

2.4 Signal to Noise Ratio

Scattered data is corrupted by means of an additive white Gaussian noise with zero mean and standard deviation computed for the v -th view as

$$\sqrt{\frac{\sum_{m=1}^M |E_v^{sca}(\mathbf{r}_m)|^2}{2M \times 10^{\frac{SNR}{10}}}} \quad (18)$$

where $E_v^{sca}(\mathbf{r}_m)$ is the scattered field at position \mathbf{r}_m under the v -th illumination and SNR is the user-defined Signal-to-Noise Ratio, in dB.

2.5 Degrees of Freedom (*DoFs*) of the Scattered Field

1. Considering the Effective Bandwidth (*EB*) approach [17], the number of Degrees of Freedom (*DoFs*) of the scattered field collected over a circular observation domain surrounding the investigation domain of side L_D is given by

$$\Gamma = 2ka \quad (19)$$

where $a = L_D \frac{\sqrt{2}}{2}$ is the radius of the smallest circle containing D ;

2. Accordingly, the number of views (V) and the number of measurement points (M) should be chosen equal (or slightly larger) to this quantity in order to collect all the available non-redundant information on the scatterer(s) embedded inside D

$$M = V \simeq \Gamma = 2ka \quad (20)$$

3. Finally, the number of unknowns that can be sought in the multi-view case is theoretically limited by

$$U = \frac{M^2}{2} = \frac{(2ka)^2}{2}. \quad (21)$$

This value will be considered as an indicator of the number of discretization cells used by the *IMSA* approach (i.e., by letting $N^{IMSA} \leq U$).

For the *BARE* approach a discretization smaller or equal to $\frac{\lambda}{10}$ will be considered.

2.6 IMSA – SOM – NIE Method

2.6.1 Stopping Criteria

The *IMSA – SOM – NIE* iterative process is stopped at the s -th step (which becomes $s = s^*$) if one of the following conditions holds true:

1. The side of the zoomed reconstruction domain for the next step ($L^{(s+1)}$) is such that:

$$\frac{|L^{(s+1)} - L^{(s)}|}{L^{(s)}} < \eta \quad (22)$$

$L^{(s)}$ being the side of the reconstruction domain at the s -th step and η a proper threshold, with $0 < \eta < 1$;

2. The maximum number of steps has been reached (i.e., $s = S$).

2.6.2 Adaptive Selection of the Number of Singular Values

According to [1] the number of selected singular values for the *SOM* Reconstruction at each *IMSA* step ($s = 1, \dots, S$) can be chosen according to one of the following strategies:

1. Non-Adaptive Strategy

$$K_{NA}^{(s)} = K_0; \quad s = 1, \dots, S \quad (23)$$

2. Adaptive Strategy [1]

$$\begin{cases} K_A^{(s)} = \arg \left\{ \min_{K^{(s)}} \left[\frac{\sum_{m=1}^M \chi_m^{(s)}}{\sum_{m=1}^K \chi_m^{(s)}} - \alpha \right] \right\} \\ \text{subject to } \frac{\sum_{m=1}^K \chi_m^{(s)}}{\sum_{m=1}^M \chi_m^{(s)}} - \alpha > 0 \end{cases} \quad (24)$$

where $\chi_m, m = 1, \dots, M$, are the singular values of the scattering operator (external Green's matrix) and $0 \leq \alpha \leq 1$ is a user-defined threshold (to be properly tuned).

2.7 Adaptive Computation of the NIE Regularization Parameter

The regularization parameter in the *NIE* formulation can be set according to the following strategies

1. Non-Adaptive Strategy:

$$\beta_{NA}^{(s)} = \beta_0; \quad s = 1, \dots, S \quad (25)$$

2. Adaptive Strategy: the coefficient β is computed as a function of the maximum of the internal operator with unit input

$$\beta_A^{(s)} = \gamma \times \max_{\mathbf{r} \in D^{(s)}} \left| \int_{D^{(s)}} G^{(s)}(\mathbf{r}, \mathbf{r}') d\mathbf{r}' \right| \quad (26)$$

where γ is a user-selected multiplicative factor (to be properly tuned).

3 Preliminary Software Validation

3.1 Goal

- Verify that the SW implementing the *BARE – SOM – NIE* and *IMSA – SOM – NIE* methods are correctly working.

Note that the parameters are not calibrated, this test has the unique goal of verifying the correct integration of the inverse solver with the ELEDIA tools managing the *IMSA* and the solution of the forward problem.

3.2 Parameters

Investigation domain (D)

- Side: $L_D = 6.0 [\lambda]$;

Measurement setup

- Views
 - Type: plane wave with unitary magnitude;
 - Frequency: $f = 300$ [MHz];
 - Wavelength: $\lambda = 1.0$ [m];
 - Number of DOFs: $\Gamma = 2ka = 2k \left(L_D \frac{\sqrt{2}}{2} \right) = 4\frac{\pi}{\lambda} \left(L_D \frac{\sqrt{2}}{2} \right) \simeq 53.25$;
 - Number of views: $V = 53$;
 - Direction: $\varphi_v = (v - 1) \frac{360}{V}$; $v = 1, \dots, V$;
- Measurement points
 - Radius: $\rho = a = \left(L_D \frac{\sqrt{2}}{2} \right) = 4.24 [\lambda]$;
 - Number of probes: $M = 53$;
 - Location: $(x_m, y_m) = (\rho \cos((m - 1) \frac{2\pi}{M}), \rho \sin((m - 1) \frac{2\pi}{M}))$; $m = 1, \dots, M$;

Scatterer

- Type: “Austria Profile”
- Dielectric characteristics: $\epsilon_r = 2.5$, $\sigma = 0.0$ [S/m] $\rightarrow \tau = 1.5$;

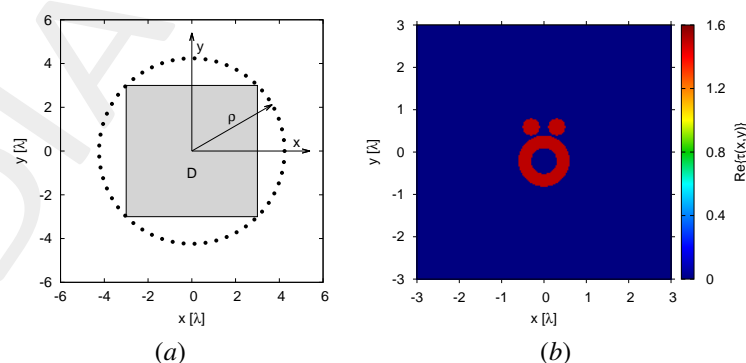


Figure 1: Software Validation (“Austria Profile”, $\tau = 1.5$) - (a) Imaging scenario and (b) actual dielectric profile.

Forward solver (MoM)

- Discretization: $N^{fwd} = 65 \times 65 = 4225$;
- Side of each cell: $l^{fwd} \simeq 0.092 [\lambda]$;

Inverse solver

1. BARE – SOM – NIE

- Discretization: $N = 64 \times 64 = 4096$;
- Side of each cell: $l = 0.094 [\lambda]$;
- Number of singular values: $K = 15$ (non-adaptive);
- Number of Fourier bases: $MF = \frac{\sqrt{N}}{2} = 32$ (standard SOM);
- NIE regularization parameter: $\beta = 6.0$ (non-adaptive);
- Number of iterations: $I = 100$.

2. IMSA – SOM – NIE

- Number of retrievable unknowns: $U = \frac{(2ka)^2}{2} = 4\pi^2 \left(\frac{L}{\lambda}\right)^2 = 1420$;
- Discretization: $N = 36 \times 36 = 1296$;
- Side of each cell @ $s = 1$: $l_{s=1} = 0.17 [\lambda]$;
- Maximum number of steps: $S = 2$;
- Stop criterion: maximum number of steps.
- Selection of the singular values: non-adaptive;
- Number of singular values: $K = 15$ (non-adaptive);
- Number of Fourier bases: $MF = \frac{\sqrt{N}}{2} = 18$ (standard SOM);
- NIE regularization parameter: $\beta = 6.0$ (non-adaptive);
- Number of iterations: $I = 100$.

Signal to noise ratio

- $SNR = \{10; 20; 40; 60\}$ [dB].

3.3 Results

IMSA – SOM – NIE vs. BARE – SOM – NIE: Final reconstructions

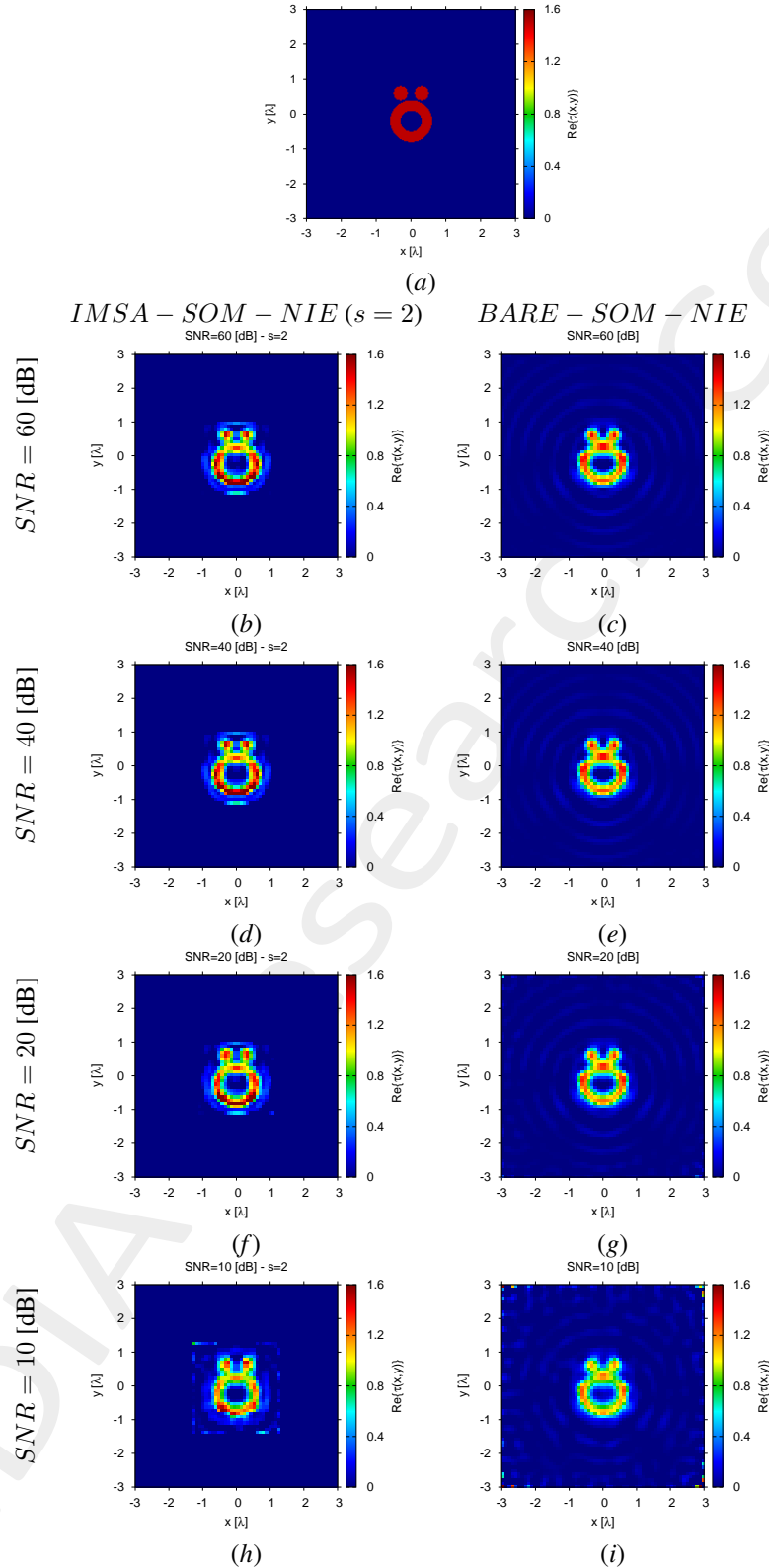


Figure 2: Software Validation (“Austria Profile”, $\tau = 1.5$) - (a) Actual and (b)-(i) retrieved contrast by the *IMSA – SOM – NIE* and *BARE – SOM – NIE* methods under several noise levels.

IMSA – SOM – NIE: Intermediate Reconstructions

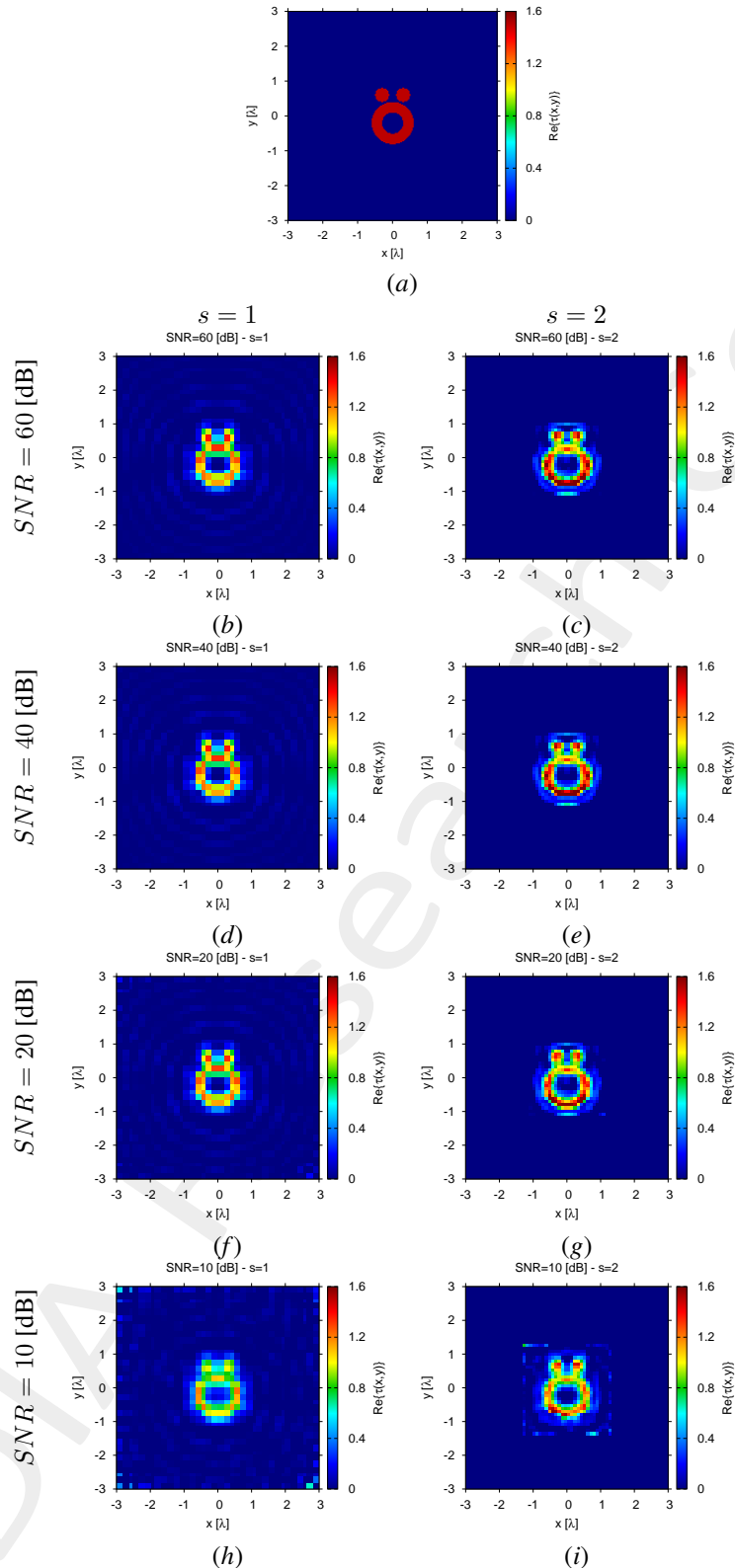


Figure 3: Software Validation (“Austria Profile”, $\tau = 1.5$) - (a) Actual and (b)-(i) intermediate retrieved contrast by the *IMSA – SOM – NIE* under several noise levels.

IMSA – SOM – NIE vs. BARE – SOM – NIE: Reconstruction Errors and Times

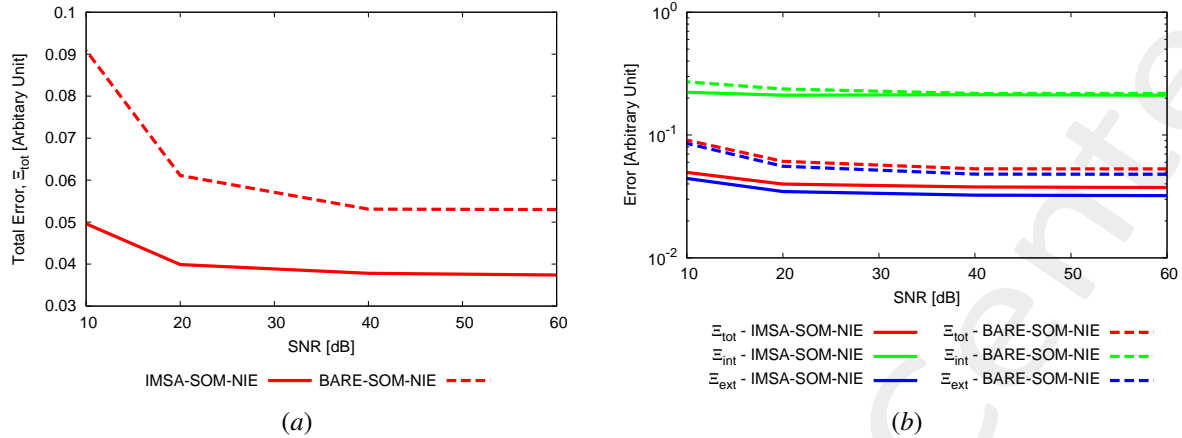


Figure 4: Software Validation (“Austria Profile”, $\tau = 1.5$) - Reconstruction errors and times for the *IMSA – SOM – NIE* and *BARE – SOM – NIE* methods under several noise levels.

IMSA – SOM – NIE					BARE – SOM – NIE				
SNR [dB]	Step, s	Ξ_{tot}	Ξ_{int}	Ξ_{ext}	Δt [sec]	Ξ_{tot}	Ξ_{int}	Ξ_{ext}	Δt [sec]
60	2	3.74×10^{-2}	2.11×10^{-1}	3.21×10^{-2}	47	5.30×10^{-2}	2.18×10^{-1}	4.79×10^{-2}	61
40	2	3.78×10^{-2}	2.13×10^{-1}	3.24×10^{-2}	47	5.31×10^{-2}	2.18×10^{-1}	4.81×10^{-2}	61
20	2	3.99×10^{-2}	2.11×10^{-1}	3.47×10^{-2}	47	6.11×10^{-2}	2.37×10^{-1}	5.57×10^{-2}	61
10	2	4.96×10^{-2}	2.23×10^{-1}	4.43×10^{-2}	47	9.09×10^{-2}	2.71×10^{-1}	8.54×10^{-2}	61

Table I: Software Validation (“Austria Profile”, $\tau = 1.5$) - Reconstruction errors and times for the *IMSA – SOM – NIE* and *BARE – SOM – NIE* methods under several noise levels.

3.4 Conclusions

- The reported results indicate the correct sw implementation/integration of both *BARE – SOM – NIE* and *IMSA – SOM – NIE*;
- Even if the parameters have not been yet calibrated, the *IMSA – SOM – NIE* shows a non negligible advantage over the *BARE – SOM – NIE* in terms of reconstruction error and execution time.

References

- [1] G. Oliveri, Y. Zhong, X. Chen, and A. Massa, "Multiresolution subspace-based optimization method for inverse scattering problems," *J. Opt. Soc. Am. A*, vol. 28, no. 10, pp. 2057-2069, Oct. 2011.
- [2] X. Ye, L. Poli, G. Oliveri, Y. Zhong, K. Agarwal, A. Massa, and X. Chen, "Multi-resolution subspace-based optimization method for solving three-dimensional inverse scattering problems," *J. Opt. Soc. Am. A*, vol. 32, no. 11, pp. 2218-2226, Nov. 2015.
- [3] T. Moriyama, G. Oliveri, M. Salucci, and T. Takenaka, "A multi-scaling forward-backward time-stepping method for microwave imaging," *IEICE Electronics Express*, vol. 11, no. 16, pp. 20140569(1-10), Aug. 2014.
- [4] N. Anselmi, G. Oliveri, M. Salucci, and A. Massa, "Wavelet-based compressive imaging of sparse targets," *IEEE Trans. Antennas Propag.*, vol. 63, no. 11, pp. 4889-4900, Nov. 2015.
- [5] M. Salucci, G. Oliveri, and A. Massa, "GPR prospecting through an inverse scattering frequency-hopping multi-focusing approach," *IEEE Trans. Geosci. Remote Sens.*, vol. 53, no. 12, pp. 6573-6592, Dec. 2015.
- [6] T. Moriyama, M. Salucci, T. Tanaka, and T. Takenaka, "Image reconstruction from total electric field data with no information on incident field," *J. Electromagn. Waves Appl.*, 2016.
- [7] M. Salucci, L. Poli, and A. Massa, "Advanced multi-frequency GPR data processing for non-linear deterministic imaging," *Signal Proc.*, vol. 132, pp. 306-318, Mar. 2017.
- [8] M. Salucci, L. Poli, N. Anselmi, and A. Massa, "Multifrequency particle swarm optimization for enhanced multiresolution GPR microwave imaging," *IEEE Trans. Geosci. Remote Sens.*, vol. 55, no. 3, pp. 1305- 1317, Mar. 2017.
- [9] N. Anselmi, G. Oliveri, M. A. Hannan, M. Salucci, and A. Massa, "Color compressive sensing imaging of arbitrary-shaped scatterers," *IEEE Trans. Microw. Theory Techn.*, vol. 65, no. 6, pp. 1986-1999, Jun. 2017.
- [10] G. Oliveri, M. Salucci, N. Anselmi, and A. Massa, "Compressive sensing as applied to inverse problems for imaging: theory, applications, current trends, and open challenges," *IEEE Antennas Propag. Mag.*, vol. 59, no. 5, pp. 34-46, Oct. 2017.
- [11] M. Salucci, A. Gelmini, L. Poli, G. Oliveri, and A. Massa, "Progressive compressive sensing for exploiting frequency-diversity in GPR imaging," *J. Electromagn. Waves Appl.*, vol. 32, no. 9, pp. 1164- 1193, 2018.
- [12] G. Oliveri, M. Salucci, and N. Anselmi, "Tomographic imaging of sparse low-contrast targets in harsh environments through matrix completion," *IEEE Trans. Microw. Theory Techn.*, vol. 66, no. 6, pp. 2714-2730, Jun. 2018.
- [13] M. Salucci, L. Poli, and G. Oliveri, "Full-vectorial 3D microwave imaging of sparse scatterers through a multi-task Bayesian compressive sensing approach," *J. Imaging*, vol. 5, no. 1, pp. 1-24, Jan. 2019.
- [14] M. Salucci, G. Oliveri, and A. Massa, "Real-time electrical impedance tomography of the human chest by means of a learning-by-examples method," *IEEE J. Electromagn., RF, Microw. Med. Biol.*, vol. 3, no. 2, pp. 88-96, Jun. 2019.

-
- [15] G. Oliveri, L. Poli, N. Anselmi, M. Salucci, and A. Massa, "Compressive sensing-based Born iterative method for tomographic imaging," *IEEE Trans. Microw. Theory Techn.*, vol. 67, no. 5, pp. 1753-1765, May 2019.
 - [16] I. Merunka, A. Massa, D. Vrba, O. Fiser, M. Salucci, and J. Vrba, "Microwave tomography system for methodical testing of human brain stroke detection approaches," *Int. J. Antennas Propag.*, vol. 2019, ID 4074862, pp. 1-9, 2019.
 - [17] Y. Zhong, M. Salucci, K. Xu, A. Polo, and A. Massa, "A multi-resolution contraction integral equation method for solving highly non-linear inverse scattering problems," *IEEE Trans. Microw. Theory Techn.*, vol. 68, no. 4, pp. 1234-1247, Apr. 2020.
 - [18] M. Salucci, A. Polo, K. Xu, and Y. Zhong, "A multi-resolution computational method to solve highly non-linear inverse scattering problems," *Journal of Physics: Conference Series*, vol. 1476, pp. 1-6, 2020.
 - [19] N. Anselmi, L. Poli, G. Oliveri, and A. Massa, "Iterative multi-resolution bayesian CS for microwave imaging," *IEEE Trans. Antennas Propag.*, vol. 66, no. 7, pp. 3665-3677, Jul. 2018.
 - [20] G. Oliveri, P.-P. Ding, and L. Poli "3D crack detection in anisotropic layered media through a sparseness-regularized solver," *IEEE Antennas Wireless Propag. Lett.*, vol. 14, pp. 1031-1034, 2015.
 - [21] L. Poli, G. Oliveri, P.-P. Ding, T. Moriyama, and A. Massa, "Multifrequency Bayesian compressive sensing methods for microwave imaging," *J. Opt. Soc. Am. A*, vol. 31, no. 11, pp. 2415-2428, 2014.
 - [22] G. Oliveri, N. Anselmi, and A. Massa, "Compressive sensing imaging of non-sparse 2D scatterers by a total-variation approach within the Born approximation," *IEEE Trans. Antennas Propag.*, vol. 62, no. 10, pp. 5157-5170, Oct. 2014.